JOURNAL OF MATERIALS SCIENCE 17 (1982) 677–690

Cold-worked state and annealing behaviour of austenitic stainless steel

S. W. YANG
General Electric Company, Corporate Research and Development Center, Schenectady, New York 12301, USA

J. E. SPRUIELL
Department of Chemical Metallurgical and Polymer Engineering, University of Tennessee, Knoxville, Tenessee 37916, USA

An investigation was made into the structural changes accompanying cold working and annealing treatments in seven austenitic stainless steels. The materials studied included five laboratory alloys and two commercial grades of austenitic stainless steels (types 304 and 316). X-ray line profile analysis showed that the stacking-fault energies of the seven steels ranged from 8 MJ m^{-2} to 68 MJ m^{-2}. Transmission electron microscopy (TEM) was used extensively to characterize the cold-worked and annealed states, Measurements of the resistivity change were performed to characterize the recovery and recrystallization behaviours. The cold-worked structure was found to be related to the stacking-fault energy. Dislocations tended to be arranged in planar arrays and to be confined in the original slip planes in alloys of low stacking-fault energy. Dislocation arrangement was less uniform and more random for steel of high stacking-fault energy. In none of the cases studied was the stacking-fault energy high enough to allow the cross-slip necessary to generate the dislocation cell structure often seen in other metals. Isochronal annealing of the steels reveals a distinguishable stage of resistivity recovery prior to recrystallization, which was attributed to the annihilation of vacancies and removal of carbon from the solid solution. A second stage of resistivity drop (above 500° C) resulted from recrystallization. The temperature for the start of recrystallization was found to be related to stacking-fault energy.

1. Introduction

Austenitic stainless steels generally have relatively low stacking-fault energies (less than 100 mJ m^{-2}), and deformation of these metals often leads to deformation faults, in addition to dislocations. There is considerable evidence that the dislocation cell structure commonly observed in pure metals is suppressed in alloys with low stacking-fault energies due to difficulty in dislocation cross-slip during deformation [1, 2]. The term "dislocation cells" refers to the dislocation structure resulting from dislocation cross-slip [1], a structure different from the planar dislocation arrays in metals of low stacking-fault energies. Stacking-fault energy also affects stress–corrosion properties of the austenitic stainless steels [3] through a change of cold-worked dislocation structures.

Stacking-fault energy is thought to affect the recovery and recrystallization behaviour through its effect on thermally-activated dislocation climb. Studies [4, 5] indicate that the recrystallization temperature of austenitic stainless steel is a strong function of chemical composition. The role of stacking-fault energy in determining annealing behaviour has not been established.

Early attempts to estimate stacking-fault energies of metals relied heavily on the measurement of deformation fault probability by X-ray diffraction, or the measurement of the radii of curvature of extended dislocation nodes by trans-

0022–2461/82/030677–14$04.18/0

TABLE I Chemical compositions of the austenitic stainless steels used

Type of Steel	Wt% of component elements								
	Cr	Ni	Mo	Mn	Si	P	S	N	C
304	18.2	8.75	–	1.36	0.32	0.013	–	0.0049	0.04
316	17.3	13.3	1.7	0.4	–	–	–	–	0.06
L1	18.0	14.1	–	–	–	–	–	–	0.016
L2	19.0	14.1	–	–	–	–	–	–	0.019
L3	19.0	14.0	–	–	–	–	–	–	0.006
L4	14.9	11.4	–	–	–	–	–	–	0.005
L5	18.1	20.6	–	–	–	–	–	–	0.005

mission electron microscopy (TEM). This X-ray diffraction technique was limited by the necessary assumption that the faults are always extended to their equilibrium widths. The TEM technique can only be used with metals with low stacking-fault energies [6]. The stacking-fault energies of the austenitic stainless steels are known to vary considerably depending on chemical composition [7]. Some of these are beyond the measurement power of the TEM technique.

More recent studies [7, 8] have shown that an appropriate combination of data measured from X-ray diffraction (mean square strain, fault probability) together with other measurable parameters can be applied to determine a wide range of stacking-fault energies in austenitic stainless steels.

The present investigation incorporates measurement of stacking-fault energies, a careful characterization of the cold-worked state, and the annealing behaviour of a series of austenitic stainless steels. The effect of stacking-fault energy on cold-worked structure and annealing behaviour is carefully investigated.

2. Experimental procedure

Two commercial alloys were purchased in the form of 2.5 cm diameter bars. Five laboratory alloys were vacuum-melted in a Balzer induction furnace. The raw metals used for melting were electrolytic pure iron (99.95%), commercially pure nickel (99.0% minimum*) and electrolytic pure chromium (99.9%) and pure graphite. The pressure at the start of the melting was less than 10^{-5} torr. Chemical analysis of important elements for the seven alloys is shown in Table I.

All materials were homogenized at 1050° C for 15 h, rolled, solution treated at 1050° C for one hour in argon, and water quenched. Sections of the materials were subjected to repeated rolling and annealing until a desired thickness was reached. Tensile specimens were machined from 0.05 cm sheet. The specimens had a gauge length of 5.1 cm and a width of 0.95 cm. Annealing at 1050° C for 10 min was conducted prior to tensile testing. The cross-head speed was set at 0.25 cm min^{-1} for all the tensile deformation.

Filings for X-ray diffraction were also produced from materials in the annealed condition. All the fillings were sieved through a 100 mesh sieve and were wetted with immersion oil and packed into a specimen holder. X-ray diffraction profiles from (111), (222), (002) and (004) Bragg planes were recorded with a Norelco wide-angle diffractometer using a diffracted beam monochrometer adjusted to pass only CuKβ radiation. A step-counting procedure was used for all the intensity measurements, and the intensity data were punched on paper tapes. After the tapes were converted into a punched card format, the data were analysed using an IBM 360/65 computer. The intensities were first corrected using the appropriate angular factor and subtracting a linear background. Profiles of annealed samples were also recorded to correct for the instrumental broadening using the technique developed by Stokes [9]. The Warren–Averbach method [10] was applied to separate the particle size coefficients and mean square strains. The deformation fault probabilities were derived from the change of peak separation between 111 and 200 peak maxima. Using the value of mean square strains and deformation fault probabilities, the stacking-fault energies were calculated in a manner described by Schramm and Reed [8].

Both TEM and optical microscopy were used to characterize the cold-worked state and the annealing behaviour of steels. Some effort was made to

*Impurities include 0.4% iron and 0.15% carbon.

characterize the recovery process using the X-ray profile analysis. The annealing behaviours were also monitored by measuring the changes in the electrical resistivity. For the resistivity measurements, the specimens were first subjected to a tensile deformation of 40% followed by an isochronal anneal. In the isochronal annealing, the soaking time for each temperature step was 40 min. The temperature difference between two successive steps was 30° C.

The electrical resistivity was measured using a four-probe method. Two of the probes were used to supply a constant current while the others were used to measure the potential drop across two knife edges at a fixed distance apart. All the measurements were carried out with specimens immersed in an ice bath.

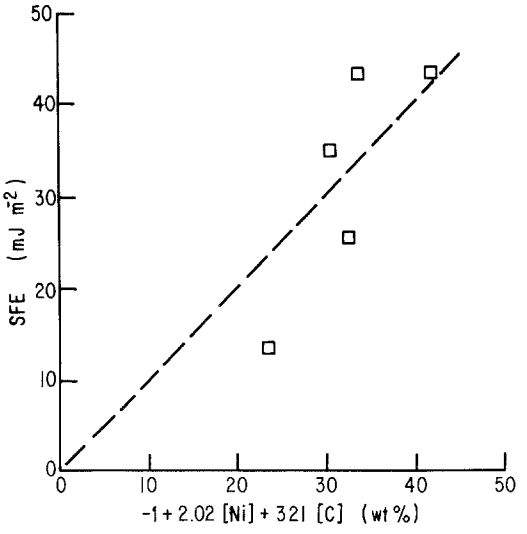

Figure 1 The relationship between the stacking-fault energy (SFE) and the equation of regression.

3. Results

3.1. Stacking-fault energy and cold-worked microstructures

Table II summarizes the values of mean square strains averaged over 5 nm distance, effective particle sizes, deformation fault probabilities and stacking-fault energies for the seven alloys under investigation. These measurements were carried out on filings as described above. The measured values of stacking-fault energy range from 8 mJ m^{-2} to 68 mJ m^{-2}.

Some traces of body-centred cubic (bcc) diffraction peaks were observed near the 111 reflections for Alloys 304 and L4. Corrections were made by folding the diffraction profiles, after correcting for background and polarization factor, about a vertical line drawn near the peak maximum. The error caused by the overlapping bcc peak was thus corrected by comparing with the tail at the other side of the maximum. This correction tended to force the diffraction profiles to be symmetric and eliminated any asymmetry caused by the twin faults. Since the Fourier sine coefficients were small throughout the investigation, it is assumed that this correction did not introduce significant error.

Since the chromium content in all the laboratory alloys is fairly constant, a multiple regression was made to reveal only relation between stacking-fault energy and contents of Ni and C. The result gives the stacking-fault energy as $-1.0 + 2.02[\mathrm{Ni}] + 321.0[\mathrm{C}]$ (contents in wt%). This is plotted in Fig. 1.

Typical dislocation structures as a function of tensile strain are shown in Fig. 2. At elongations of 20% or less, the micrographs are taken from areas in which only dislocations are present; other features which are occasionally observed are avoided in order to focus attention on the dislocation arrangements. In each column of Fig. 2, the material is the same with increasing deformation from top to bottom. The stacking-fault energy of the metal increases from left to right. Two enlarged micrographs are also shown in Fig. 3. It can be

TABLE II Mean square strain, effective size, deformation fault probability and stacking-fault energy of severn austenitic stainless steels

Alloy	Particle size (nm)	Mean square strain ($\times 10^5$)	Deformation fault probability	Stacking-fault energy (mJ m^{-2})
304	8	0.7	0.017	8
316	11	3.0	0.016	68
L1	14	2.2	0.016	25
L2	20	5.6	0.023	43
L3	18	4.5	0.023	35
L4	16	1.5	0.020	13
L5	23	4.6	0.019	43

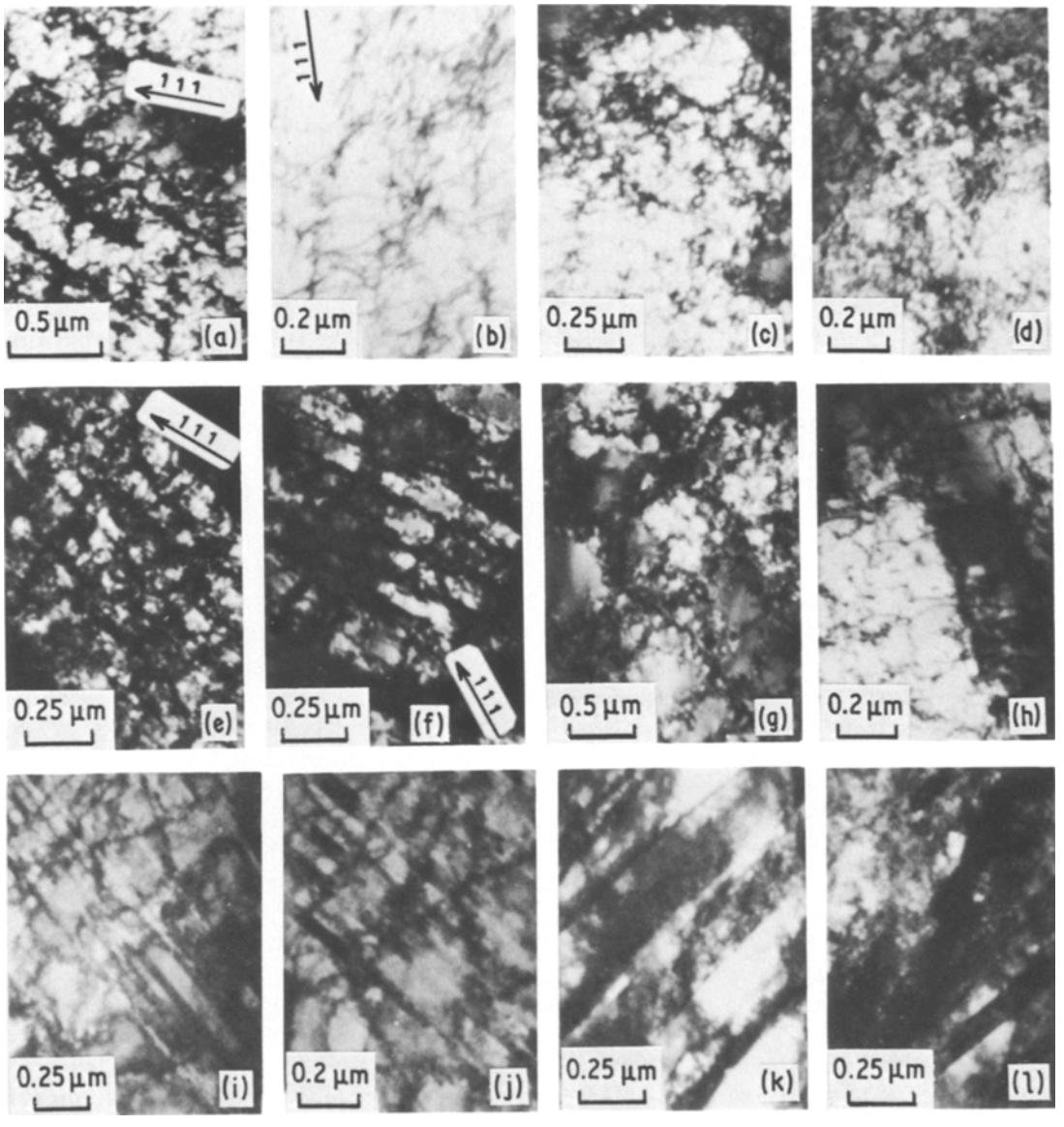

Figure 2 The cold-worked microstructures of Alloys 304, L4, L5 and 316 as a function of deformation. The material in each column, from left to right, is 304, L4, L5 and 316. The deformation for the first row (top) is 10% tensile strain, 20% tensile strain for the second row, and 40% tensile strain for the third.

seen from Figs 2 and 3 that the dislocations tend to line up in certain crystallographic directions for metals of low stacking-fault energy. Some of this directionality can be shown to be coincidental to the traces of the {1 1 1} planes. This is exemplified in Fig. 4. The dislocation arrangements tend to be more non-uniform and random for materials of higher stacking-fault energy.

The banded structures, shown in in specimens subjected to 40% extension, are also seen in specimens of low stacking-fault energy at lower deformations. These structures were attributed to overlapping stacking faults, martensite plates and microtwins by several investigators [11–13].

Detailed TEM study reveals that some of the bands are associated with strain induced martensite (see Fig. 5). This is observed most frequently in type 304 steel. Fig. 5a is the bright-field image showing the band; Fig. 5c shows the accompanying diffraction pattern. The dark-field image, Fig. 5b, is obtained using the 301 martensite spot. The presence of martensite can also be detected by X-

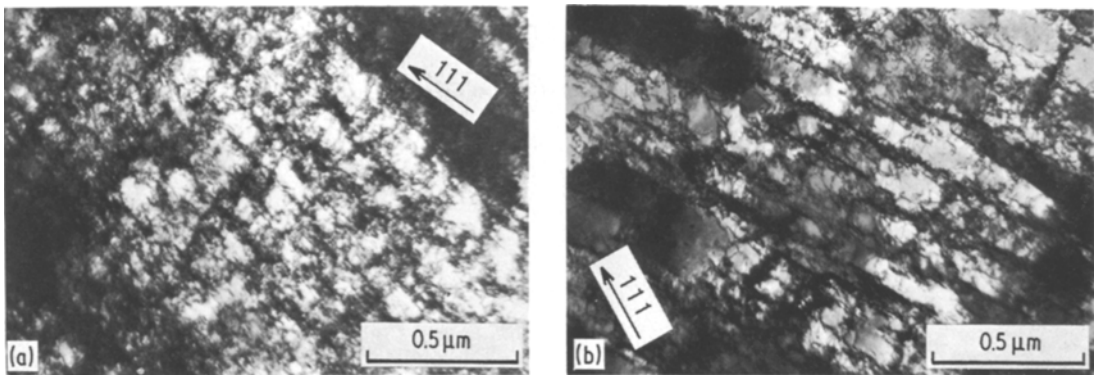

Figure 3 Cold-worked dislocation structures of (a) type 304 steel, and (b) Alloy L4, after 20% tensile deformation.

ray diffraction after 10% strain. Magnetic measurement shows that the fraction of the martensite phase is 2% under this condition. Selected-area electron diffraction also shows evidence of microtwins (see Fig. 6). Extended partial dislocations and stacking faults were also seen. No attempt was made to determine the relative amounts of twins, deformation faults and martensite.

After 40% tensile strain, the fringe contrast in the banded structure is no longer visible, probably due to a very high dislocation density. Magnetic tests show that there is some martensite present in

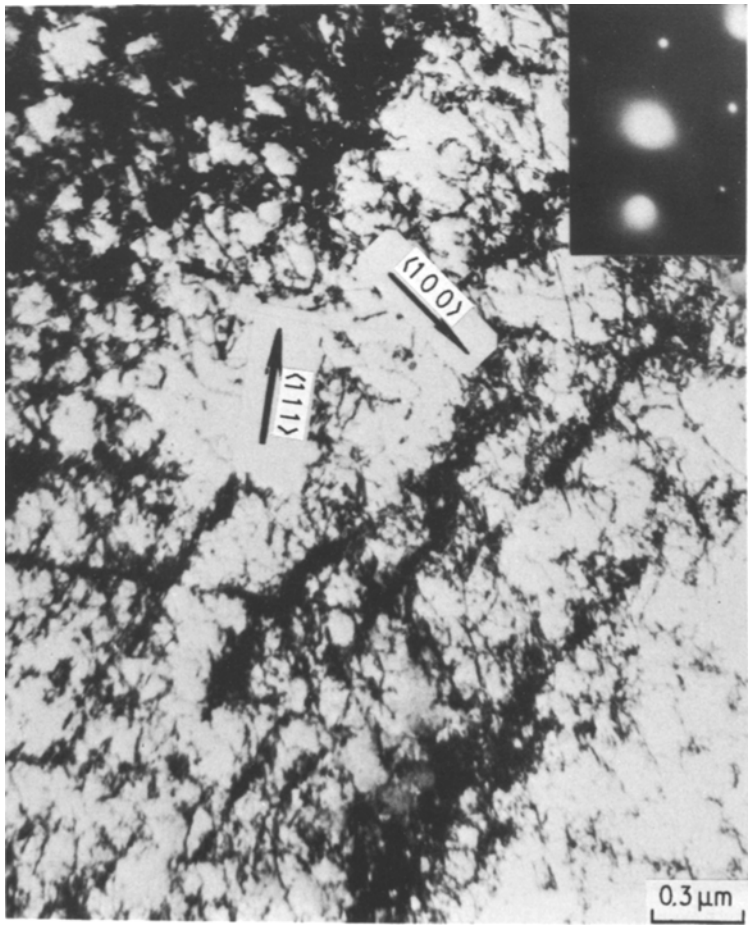

Figure 4 Microstructure of 304 steel after 10% tensile deformation, showing dislocations along the {1 1 1} trace.

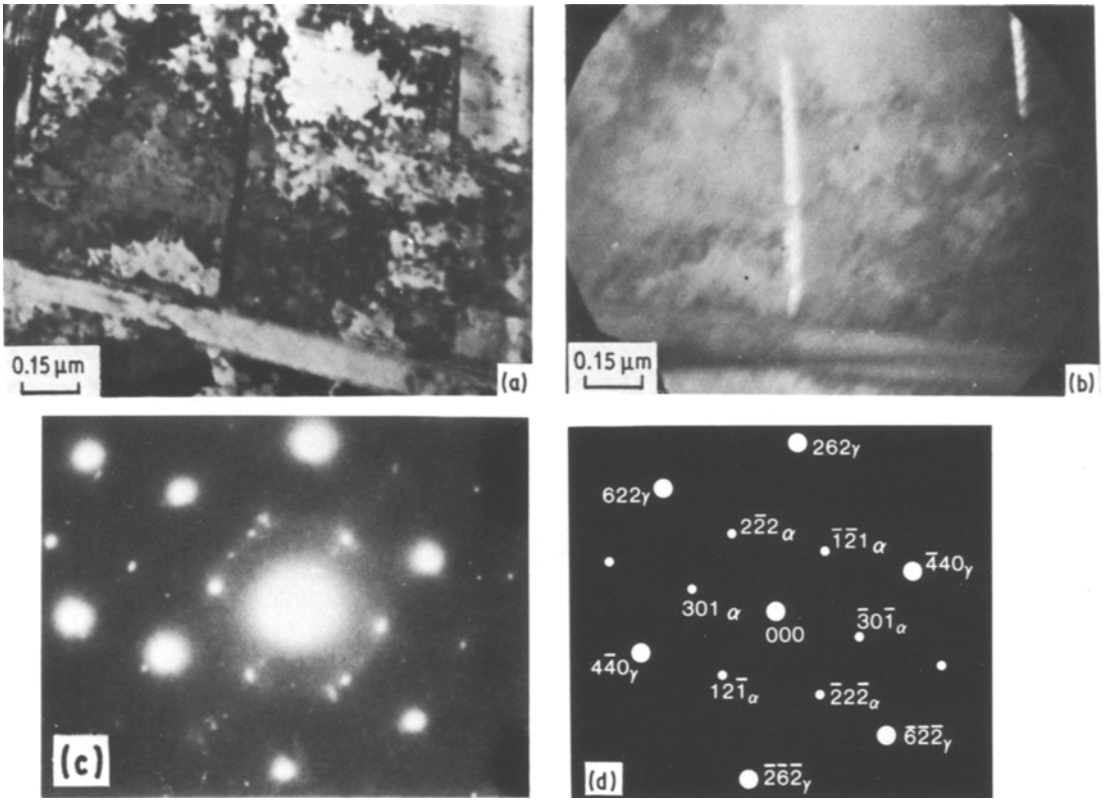

Figure 5 Microstructure of 304 steel after 10% tensile deformation, showing martensite. (a) Bright-field image, (b) dark-field image, (c) indexed diffraction pattern.

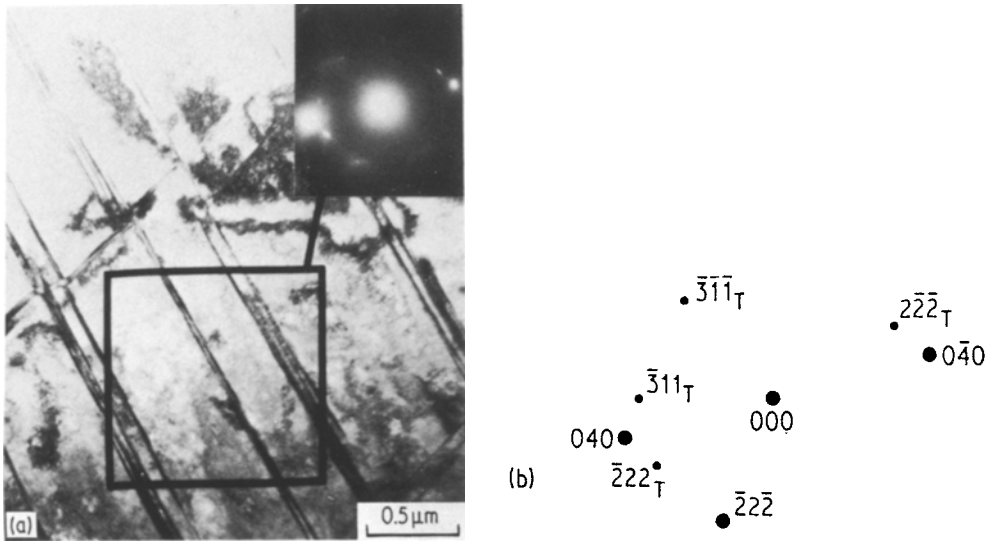

Figure 6 Microstructure of Alloy L2 after 40% tensile strain, showing the microtwins.

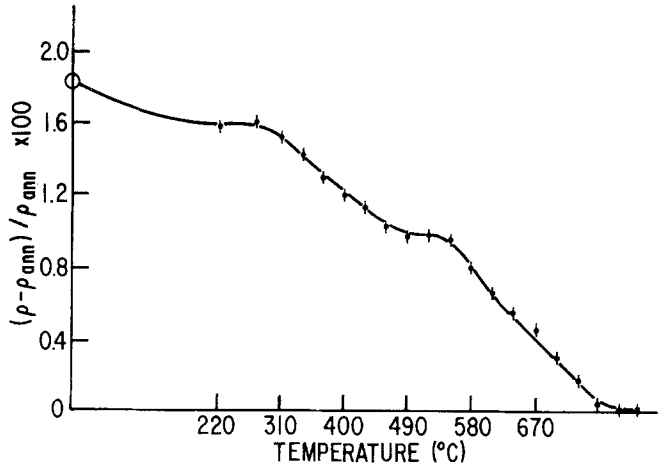

Figure 7 Resistivity change of the isochronally annealed 304 steel.

Alloys L2, L4 and 304 (approximately 1%, 3% and 4% respectively). For Alloys L2, L4 and 304, the bands are largely deformation faults, microtwins and martensite. For other alloys, the bands consist primarily of deformation faults and twins.

3.2. Annealing of the cold-worked steels

Isochronal annealing was carried out in specimens strained 40%* in tension. The results are in Figs 7–13. The ordinates represent the percentage change of resistivity using the resistivity of the fully annealed state as a reference. The relative changes of the resistivity between the cold-worked and fully annealed stainless steels vary with chemical composition. Alloy L5 is an exception case for it shows no overall change in resistivity upon annealing. Possible reasons will be discussed later.

Among most of the alloys investigated, a distinctive recovery stage can be recognized in the temperature range between about 310° C and 430° C. TEM studies of the specimens annealed through this stage show no apparent change in the cold-worked structure, as is shown in Fig. 14. The structure consists of dark bands and unresolved dislocations with no indication of the formation of dislocation cells.

Isothermal annealing studies of the Type 304 and 316 steels within the temperature range of this recovery stage allowed the activation energy for the recovery stage to be measured. The activation energy was measured to be $(56.5 \pm 12.6) \times 10^3$ J mol^{-1} and $(81.6 \pm 12.6) \times 10^3$ J mol^{-1} for 304 and 316 steel, respectively.

Between the temperature of 430° C and 500° C, the resistivity decreases very little. Another major decrease in resistivity begins at a temperature above 500° C. This last stage of change is associated with recrystallization, as shown in Fig. 15, which displays the microstructures of alloys isochronally

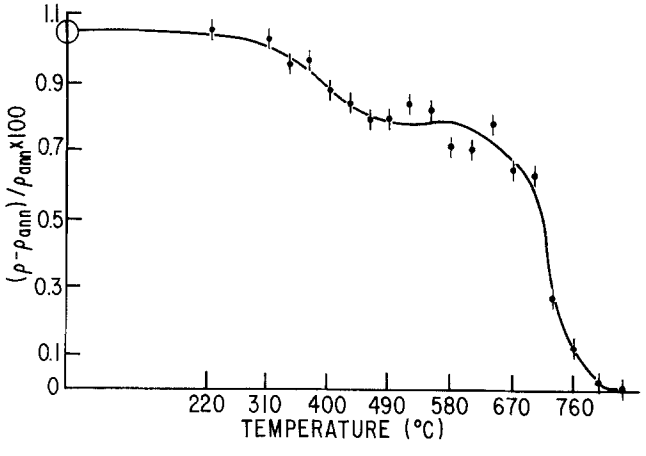

Figure 8 Resistivity change of the isochronally annealed 316 steel.

*Only 30% strain was applied to Alloy L5 due to necking.

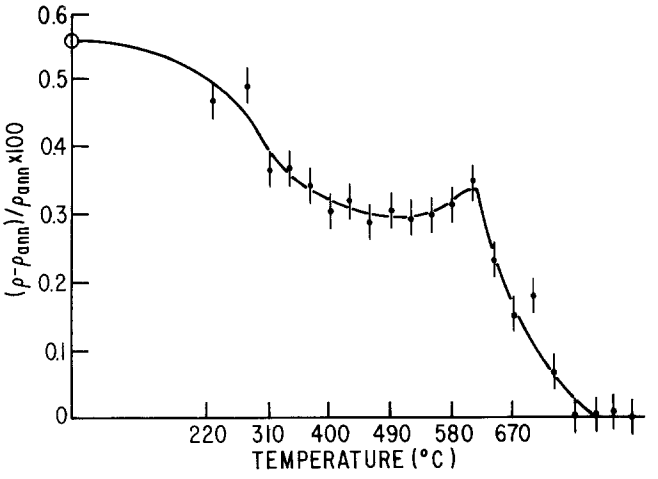

Figure 9 Resistivity change of the isochronally annealed L1 alloy.

annealed to a temperature within the second stage of resistivity decrease. Partial recrystallization is evident in Fig. 15.

4. Discussion

4.1. Stacking-fault energies and the cold-worked structure

The results on the commercial steels compare favourably with those obtained by Schramm and Reed [7]. The stacking-fault energies of the laboratory alloys are in fair agreement with those reported by Fawley *et al.* [14] using TEM. The results are also in general agreement with the trend that both Ni and C raise the stacking-fault energy of the austenitic stainless steels.

The regression analysis of stacking-fault energy with composition reveals a high coefficient associated with carbon content similar to that found by Schramm and Reed [7]. The range of carbon composition is very narrow and the possible error in determining the carbon level is relatively large compared to the range of carbon content. This makes the coefficient of carbon very sensitive to small errors. More recent analysis made by Brofman and Ansell [15], using data obtained by TEM technique, indicated a coefficient of 26 for stainless steels with higher carbon content (up to 0.29 wt%). It is, however, not clear whether all the carbon is retained in the solid solution.

The dislocation arrangement for alloys of low stacking-fault energy appears to be planar. This phenomenon is related to the difficulty in dislocation cross-slip. As cross-slip becomes difficult during plastic deformation, the dislocations are forced to stay in the original slip planes, namely {1 1 1} planes for face-centred cubic (fcc) metals.

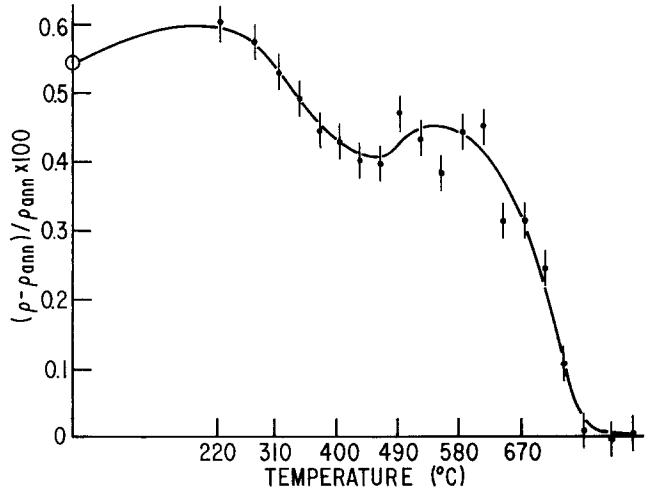

Figure 10 Resistivity change of the isochronally annealed L2 alloy.

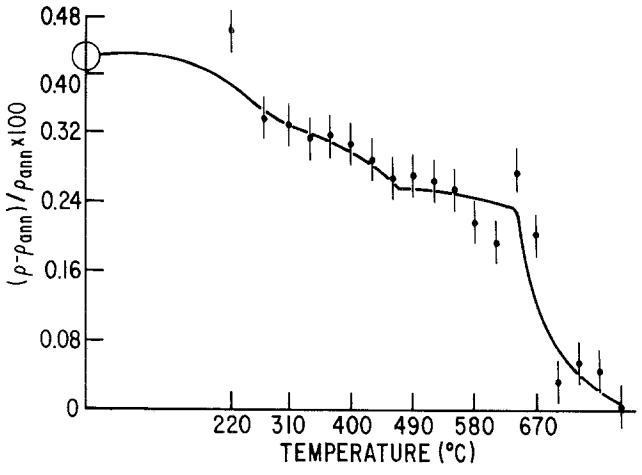

Figure 11 Resistivity change of the isochronally annealed L3 alloy.

As a result of this confinement, the dislocations tend to queue up in the {1 1 1} planes. This type of arrangement was also reported by Swann [3] in Cu–4.5 wt% Al alloy and in austenitic stainless steels. It was believed that this feature is common to metals having stacking-fault energies near the threshold value for the formation of dislocation cells. An increase of stacking-fault energy above the threshold promotes cell formation while a decrease causes the split of a perfect dislocation into two partials bounding a stacking fault. Kestenbach [16] showed that the arrangement of dislocations is also affected by local state of stress. It was noted that a tensile loading along {1 1 0} direction produced directional arrangement. Tensile loading along {1 0 0} direction reduced the width of stacking faults and promoted the formation of cell structure at 500° C. In the present study, the state of stress within each grain cannot be meaningfully determined. Nevertheless, it is reasonable to expect that the planar dislocation arrays and the banded structures are seen more often in the alloys of low stacking-fault energy.

In the alloys investigated, the dislocations tend to be more planar and uniformly distributed in alloys of lower stacking-fault energy. Formation of poorly defined dislocation cells was occasionally observed in the cold-worked 316 steels, but this could not be considered as a representative feature. The stacking-fault energies of this group of alloys are probably too low to allow extensive cross-slip at room temperature. The lack of substructure and difficulty in dislocation cross-slip has also been noted by Whelan [17, 18] in stainless steels.

4.2. Annealing behavior of the austenitic stainless steels

The lack of overall resistivity change for Alloy L5 is partly due to the fact that the specimen had only 30% tensile strain as compared to 40% strain for the others. The tensile strain for this alloy had to be reduced due to early necking of the speci-

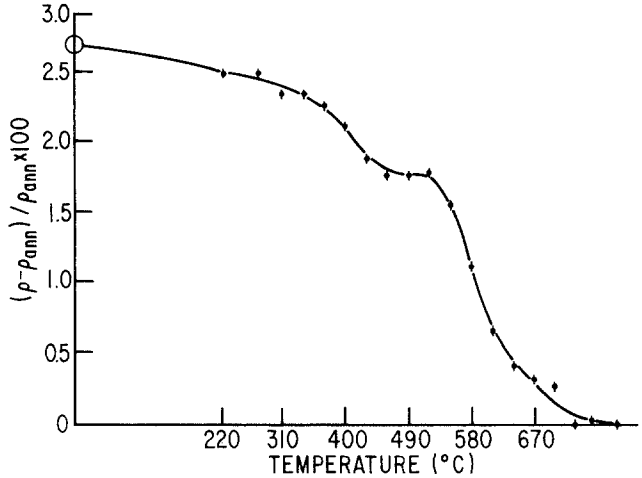

Figure 12 Resistivity change of the isochronally annealed L4 alloy.

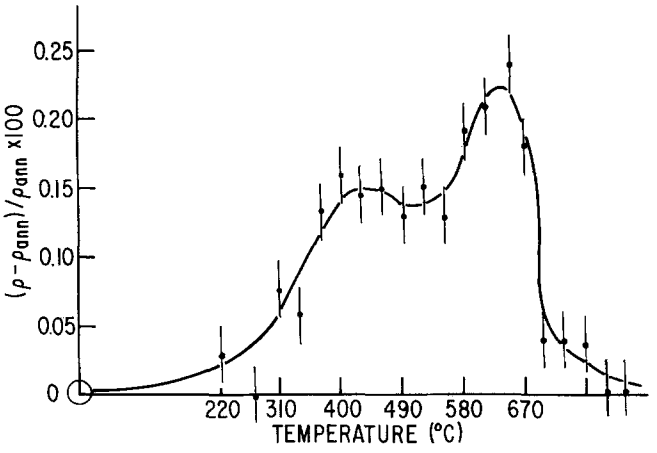

Figure 13 Resistivity change of the isochronally annealed L5 alloy.

men. Another factor to be considered is that the alloy has a high nickel content (20%). Silcock [19] has pointed out that a very high nickel content (20%–40%) in Fe–Cr–Ni alloys causes a reduction in cold-worked resistivity. In his 16Cr–20Ni steel, the cold-worked resistivity decreased by nearly 0.4% after 79% cold work. The Alloy L5 has a composition of 18.1Cr–20.6Ni which is very close to the above mentioned alloy. It was proposed that, owing to the high concentration of Ni and Cr, a few atom jumps were sufficient to form a locally ordered region, and the decrease in resistivity is due to the destruction of the short-range order [19]. The increase in resistivity during the annealing of cold-worked specimen, thus, resulting from the restoration of the short-range order. This increase was eventually off-set by the recrystallization of the alloy. The same phenomenon has been reported in Ni–10% W alloy by Ammons and Spruiell [20]. In this latter case, the short-range order was established with X-ray diffraction.

Except for the Alloy Lt, there is a noticeable recovery stage in the temperature range of about 310° C. The activation energy for this stage was measured to be $(56.5 \pm 12.6) \times 10^3$ J mol^{-1} and $(81.6 \pm 12.6) \times 10^3$ J mol^{-1} for 304 steel and 316 steel, respectively. This value is close to the activation energy of vacancy migration in Au (79.5×10^3 J mol^{-1}), Cu (100.5×10^3 J mol^{-1}) [21] and Ni (125.6×10^3 J mol^{-1}) [22], but activation

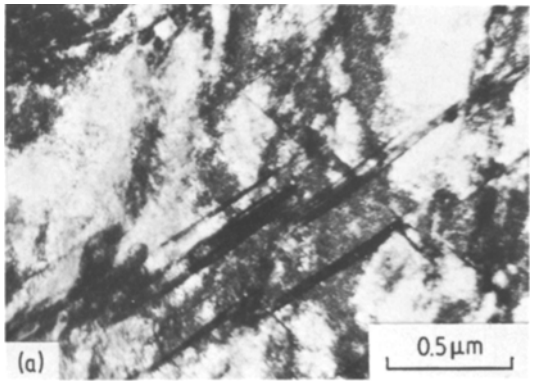

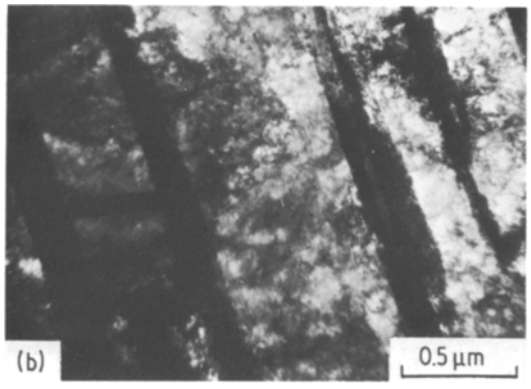

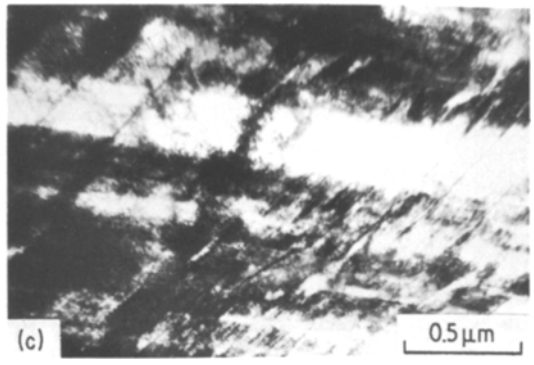

Figure 14 Microstructures of samples after 40% extension and isochronal annealing at successive temperatures to 430° C, (40 minutes at each step); (a) 304 steel, (b) L3 alloy, (c) L4 alloy.

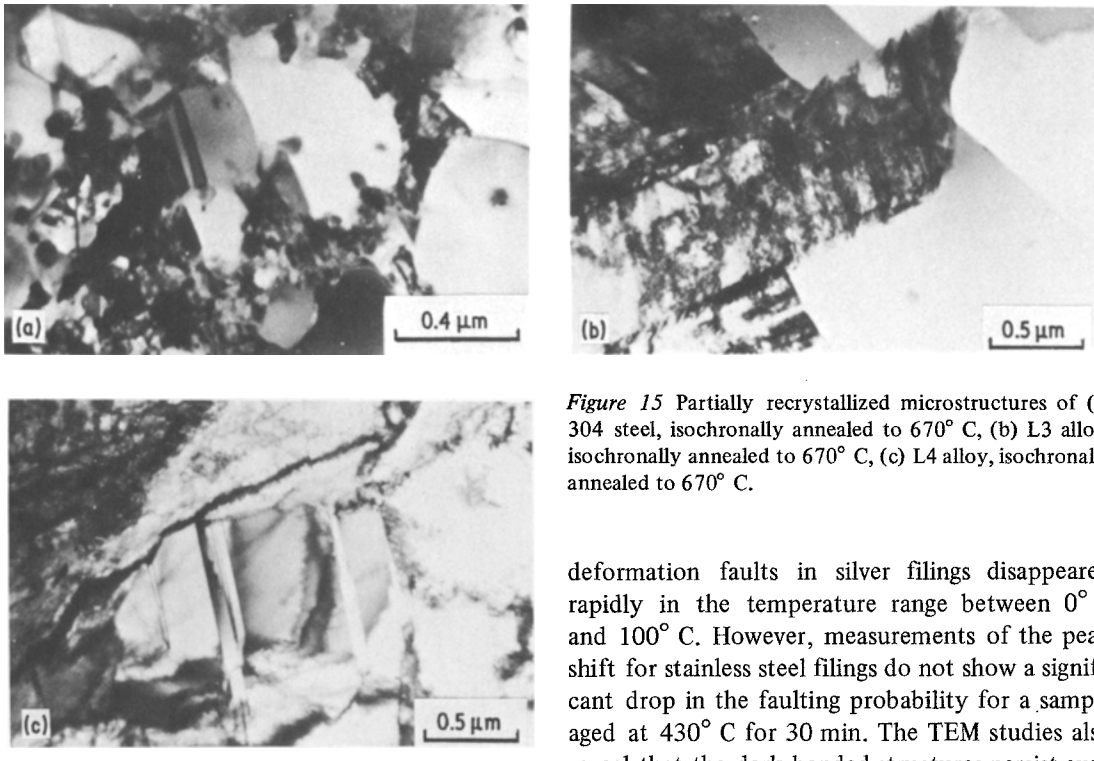

Figure 15 Partially recrystallized microstructures of (a) 304 steel, isochronally annealed to 670° C, (b) L3 alloy, isochronally annealed to 670° C, (c) L4 alloy, isochronally annealed to 670° C.

energies for vacancy migration in stainless steels are not well established. The study of Anand *et al.* [23] on irradiated steel indicated that vacancies began to be annealed out gradually in the temperature range of 260 to 550° C. It is reasonable to expect that the annihilation of point defects plays an important role in the first stage of recovery.

The limited information available on the recovery of austenitic stainless steels [24] indicated that thermally aided dislocation climb and cross-slip were difficult at temperatures below 700° C. The present study is also unable to reveal any noticeable change in dislocation arrangement for specimens aged through the first recovery stage. Moreover, if dislocation movement is largely responsible for this resistivity drop, the measured activation energy over this temperature range must be higher for 304 steel, as dislocation movement is more difficult for this alloy. This is contrary to the experimental finding. Although a minor rearrangement and elimination of dislocations cannot be ruled out, the well-known recovery process taking place by rearranging the dislocations into cells does not appear to be important during this stage of recovery.

Annealing of the deformation faults is another possibility. Wagner [25] has shown that the deformation faults in silver filings disappeared rapidly in the temperature range between 0° C and 100° C. However, measurements of the peak shift for stainless steel filings do not show a significant drop in the faulting probability for a sample aged at 430° C for 30 min. The TEM studies also reveal that the dark banded structures persist even in specimens aged to temperatures high enough for partial recrystallization. This indicates that the elimination of stacking faults is gradual and is not solely responsible for the appearance of a distinctive resistivity drop.

Carbon coming out of its interstitial position and clustering at the dislocations or other type of defects can also contribute to a decrease in resistivity. A study by Anand *et al.* [23] showed that carbon gained mobility at as low a temperature as 160° C in a 304 steel. Fujita and Damask [26], in studying an irradiated plain carbon steel, indicated that the carbon began to be trapped by vacancies at a temperature of 50° C. Similar behaviour was identified by Garafalo *et al.* [27]. They proposed a strain ageing at 480° C followed by ageing at 700° C for improving the creep strength of a 316 steel. The heat treatment at 480° C was suggested due to the higher strength indicated by hot hardness results. Their TEM study on the 316 steel, prestrained 9% and treated for 24 h at 480° C, showed very fine precipitate particles associated with the dislocation; these particles presumably grew larger on annealing at 700° C. In the work of Fujita and Damask [26], on a plain carbon steel, a resistivity step starting at about 260° C was attributed to the precipitation of Fe_3C phase. A similar reason is probable for the case of stainless

Figure 16 316 steel isothermally annealed at 800° C for 15 minutes which was subjected to a tensile pre-strain of 40%.

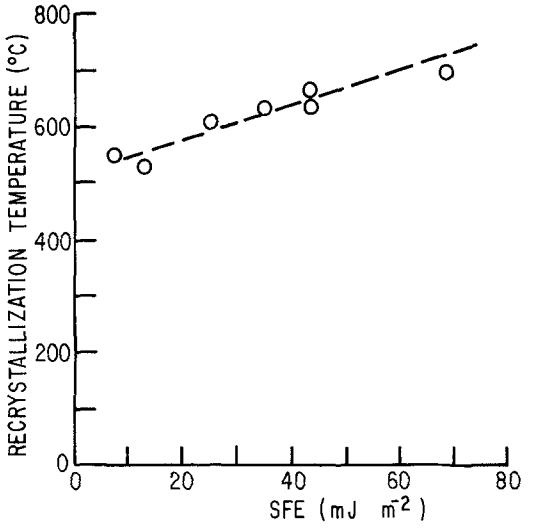

Figure 17 Temperature for the start of recrystallization as a function of stacking-fault energy.

steels at a slightly higher temperature. Therefore, it is reasonable to expect that carbon should come out of its solid solution in this temperature range.

With these indirect evidences, it is believed that the resistivity step between 310° C and 430° C is mainly associated with vacancy migration and removal of carbon from the solid solution.

The resistivity drop in a temperature range above 500° C is, in most cases, better defined than the stage between 310 and 430° C. Electron microscopy shows that recrystallization is associated with this stage in all the alloys.

In studying the partially recrystallized specimens, evidence can be found that the recrystallized grains are associated with the former grain boundary already existing in the cold-worked condition. Fig. 16 gives an excellent example. The former grain boundary is decorated with carbide particles and is seen to be adjacent to the recrystallized grains. The mechanisms for the nucleation of the recrystallized grain is not clear.

The temperatures for the start of the recrystallization, according to the isochronal resistivity measurements, show a remarkable difference. Referring to the isochronal annealing curves, a horizontal line can be drawn to approximate the resistivity change between 450 and 550° C. If the slope, representing the resistivity drop during recrystallization, is extrapolated to intersect the horizontal line, a point can be defined corresponding to the temperature for the initiation of the recrystallization. If the recrystallization temperature is defined as the temperature of an experimental measurement nearest to the above-mentioned point, the temperature of the start of recrystallization can be plotted against the stacking-fault energy of the corresponding alloys (Fig. 17). The resulting correlation indicates that the recrystallization temperature is influenced by the stacking-fault energy. Herrera *et al.* [5] revealed a similar trend for two austenitic stainless steels with different stacking-fault energy. They believed that the metal with lower stacking-fault energy recrystallized at a lower temperature due to a greater stored energy resulting from a higher strain hardening rate of the metals. A recent study of Kestenbach [16] indicated, in 304 crystals, that a change in dislocation arrangement was responsible for a change in recrystallization temperatures in the same steel. The different dislocation structures were produced by loading the crystals along ⟨100⟩ or ⟨110⟩ axes. Loading along the ⟨100⟩ axis produced dislocation cells which were a stable low-energy configuration and raised the recrystallization temperature.

As discussed before, the lowering of the stacking-fault energy tends to promote evenly distributed dislocation structures or, in other words, to retard

the formation of dislocation cells. Also, a lower stacking-fault energy tends to increase the strain hardening rate which, in turn, increases the amount of mechanical work required to achive the same plastic strain. Assuming a constant proportion of mechanical work is stored in the deformed matrix, a higher strain hardening rate should lead to a higher stored energy. Both the proposals by Herrera *et al.* and by Kestenbach point to the same conclusion, that lower stacking-fault energy leads to lower recrystallization temperature. This is in excellent agreement with the present investigation. Attempts to correlate the recrystallization temperature with the strain hardening rate yields a poor correlation in this study. This seems to indicate that the relationship between recrystallization temperature and the strain hardening rate is not straightforward.

The start of the recrystallization does not appear to be severely affected by the carbon content in this group of alloys. However, the precipitation of fine carbide is expected to have some effect on the growth rate of the recrystallized grains through its effect on the mobility of the moving recrystallizing boundary.

It must be noted that the present measurements are only effective in determining the onset temperatures for recrystallization. The growth rate of the recrystallizing grain and change caused by different carbon content must be determined through a rigorous analysis of the nucleation and growth kinetics.

5. Conclusion

The following conclusions can be made as a result of this study:

(a) The stacking-fault energies of the austenitic stainless steels are generally low; this prevents the formation of a well defined dislocation cell structure in the cold-worked state. The dislocation arrangement tends to be more planar and confined to the slip planes for steels of lower stacking-fault energy. In the steels of higher stacking-fault energy, the arrangement tends to be less uniform, approaching a cell structure.

(b) The recovery processes occurring in the austenitic stainless steels do not involve a major rearrangement of dislocations for specimens aged at temperatures below 500° C for short duration (40 minutes).

(c) A resistivity recovery step between 310° C–430° C is believed to result from annihilation of point defects and removal of carbon from solid solution.

(d) The temperature for the start of the recrystallization is affected by the stacking-fault energy. An increase of the stacking-fault energy leads to a higher recrystallization temperature.

Acknowledgement

This work is based on the dissertation completed at University of Tennessee as a partial fulfillment of PhD degree requirements. The program was supported by the Energy Research & Development Adminstration (now Department of Energy), No. AT-(40-1)-4044. A critical review from T. M. Devine is also appreciated.

References

1. P. R. SWANN, "Electron microscopy and Strength of Crystals" (Wiley Interscience, New York, 1963) p. 131.
2. P. B. HIRSCH, "Internal Stresses and Fatigue in Metals", (Elsevier, New York, 1958) p. 139.
3. P. R. SWANN, *Corrosion* **19** (1963) 102.
4. A. GROT and J. E. SPRUIELL, *Met. Trans.* **6A** (1975) 2023.
5. E. J. HERRERA, B. RAMASWAMY and D. R. F. WEST, *J. Iron Steel Inst.* **221** (1973) 229.
6. T. W. CHRISTIAN and P. R. SWANN, "Alloying Behavior and Effects in Concentrated Solid Solutions", AIME Conferences, Vol. 29, (Gordon and Breach, Cleveland, Ohio, 1965) p. 105.
7. R. E. SCHRAMM and R. P. REED, *Met. Trans.* **6** (1975) 1345.
8. R. P. REED and R. E. SCHRAMM, *J. Appl. Phys.* **45** (1974) 4705.
9. A. R. STOKES, *Proc. Phys. Soc. Lond.* **61** (1948) 382.
10. B. E. WARREN, "X-ray Diffraction", (Addison-Wesley Inc., New York, 1969).
11. B. WEISS and R. STICKLER, *Met. Trans.* **3** (1972) 851.
12. J. SPRUIELL, J. A. SCOTT, C. S. ARY and R. J. HARDIN, *ibid.* **4** (1973) 1533.
13. J. A. VENABLES, *Phil. Mag.* 7 (1962) 35.
14. R. F. FAWLEY, M. A. QUADER and R. A. DODD, *Trans. TMS-AIME* **242** (1968) 771.
15. P. J. BROFMAN and G. S. ANSELL, *Met. Trans.* **9A** (1978) 879.
16. H. J. KESTENBACH, *Met. Trans.* **8A** (1962) 213.
17. M. H. WHELAN, in "The Physics of Metals, Pt. 2", edited by P. B. Hirsch, Cambridge University Press, Cambridge (1975) p. 126.
18. M. J. WHELAN, *Proc. Roy. Soc.* **A249** (1959) 114.
19. J. M. SILCOCK, *Metal. Sci. J.* **5** (1971) 182.
20. A. M. AMMONS and J. E. SPRUIELL, *J. Appl. Phys.* **39** (1968) 3682.
21. A. C. DAMASK and G. J. DIENES, "Point Defects in Metals" (Gorden and Breach, London, 1963) p. 307

22. C. P. FLYNN, "Point Defects and Diffusion", (Clarendon Press, Oxford, 1972) p. 336.
23. M. S. ANAND, B. M. PANDE and R. P. AGARWALA, *J. Nucl. Mater.* **58** (1975) 117.
24. J. MOTEFF, *Acta Metal.* **21** (1973) 1269.
25. C. N. J. WAGNER, *ibid.* **5** (1957) 477.
26. F. E. FUJITA and A. C. DAMASK, *ibid.* **12** (1964) 331.
27. F. GARAFALO, F. VON GEMMINGEN and W. F. DOMIS, *Trans. ASM* **54** (1961) 430.

Received 22 January
and accepted 18 June 1981